

UCLA

UCLA Previously Published Works

Title

Building Structures Atom by Atom via Electron Beam Manipulation

Permalink

<https://escholarship.org/uc/item/3705k0cf>

Journal

SMALL, 14(38)

ISSN

1613-6810

Authors

Dyck, Ondrej
Kim, Songkil
Jimenez-Izal, Elisa
et al.

Publication Date

2018

DOI

10.1002/smll.201801771

Peer reviewed

Building Structures Atom by Atom via Electron Beam Manipulation

Ondrej Dyck,* Songkil Kim, Elisa Jimenez-Izal, Anastassia N. Alexandrova, Sergei V. Kalinin, and Stephen Jesse

Building materials from the atom up is the pinnacle of materials fabrication. Until recently the only platform that offered single-atom manipulation was scanning tunneling microscopy. Here controlled manipulation and assembly of a few atom structures are demonstrated by bringing together single atoms using a scanning transmission electron microscope. An atomically focused electron beam is used to introduce Si substitutional defects and defect clusters in graphene with spatial control of a few nanometers and enable controlled motion of Si atoms. The Si substitutional defects are then further manipulated to form dimers, trimers, and more complex structures. The dynamics of a beam-induced atomic-scale chemical process is captured in a time-series of images at atomic resolution. These studies suggest that control of the e-beam-induced local processes offers the next step toward atom-by-atom nanofabrication, providing an enabling tool for the study of atomic-scale chemistry in 2D materials and fabrication of predefined structures and defects with atomic specificity.

1. Introduction

Fabrication of matter atom by atom remains a long-standing dream and ultimate goal of nanotechnology, following the famous challenge by Feynman 58 years ago.^[1] For 30 years, the atom-by-atom fabrication remained the province of visionary thinking and science fiction, inspiring but seemingly unachievable given the then available fabrication tools. The situation changed drastically upon the introduction of scanning tunneling microscopy (STM) by Binnig and Rohrer^[2–4] and subsequently

STM-based atomic fabrication by Eigler.^[5–8] This advancement immediately riveted the attention of both the scientific and general community worldwide, launching the era of nanotechnology. It also started the developments of technologies based on combined STM and surface science methods, ultimately leading to the development of single-atom qubit devices.^[9–11]

Despite the remarkable progress in STM-based atomic fabrication, the fabrication process remains slow and requires complex surface science approaches to establish and maintain atomically clean surfaces. This process further requires a complex technological cycle to integrate single-atom devices with the classical semiconductor technologies. Correspondingly, the development process remained slow and required large capital investments to even begin the development. Thus, alternative methods for atom-by-atom fabrication are of interest.

Another candidate for single-atom movement has recently been identified and, while this field of inquiry is still in its nascent stages, it shows some promise. In recent years, the ever-growing body of work in high-resolution scanning transmission electron microscopy has illustrated the potential of the electron beam to induce local atomic-scale changes in materials microstructure that can be immediately visualized.^[12–19] It was then proposed that the e-beam can be used for fabrication of atomic-scale structures.^[20–28]

Dr. O. Dyck, Dr. S. V. Kalinin, Dr. S. Jesse
The Center for Nanophase Materials Sciences
Oak Ridge National Laboratory
Oak Ridge, TN 37831, USA
E-mail: ondrej.dyck@gmail.com, dyckoe@ornl.gov


Dr. O. Dyck, Dr. S. V. Kalinin, Dr. S. Jesse
The Institute for Functional Imaging of Materials
Oak Ridge National Laboratory
Oak Ridge, TN 37831, USA

Prof. S. Kim
School of Mechanical Engineering
Pusan National University
Busan 46241, South Korea

Dr. E. Jimenez-Izal
Department of Chemistry and Biochemistry
University of California
Los Angeles, Los Angeles, CA 90095-1569, USA

Dr. E. Jimenez-Izal, Prof. A. N. Alexandrova
Kimika Fakultatea
Euskal Herriko Unibertsitatea (UPV/EHU)
and Donostia International Physics Center (DIPC)
P. K. 1072, 20080 Donostia, Euskadi, Spain

Prof. A. N. Alexandrova
California NanoSystems Institute
570 Westwood Plaza, Building 114, Los Angeles, CA 90095, USA

 The ORCID identification number(s) for the author(s) of this article can be found under <https://doi.org/10.1002/sml.201801771>.

DOI: 10.1002/sml.201801771

Following these predictions, Susi et al.^[18,29] demonstrated controllable e-beam-induced movement of a single Si a short distance through the graphene lattice. This was accomplished through spot irradiation of a C atom adjacent to a dopant Si. Occasionally the C atom receives a large enough impact (≈ 15 eV) from the beam to induce a bond reversal where the Si and C switch places in the lattice. Repeating this technique, an atom may be controllably moved step by step through the graphene lattice. They also calculated the energy required for various processes involved in atomic motion and the creation of point defects. This built upon previous, related work,^[13,19,30,31] and was expanded upon by additional studies by Robertson et al.^[32–36] and others^[17,37–39] which served to clarify various atomic-scale processes and transformations in graphene. Dyck et al.^[40] has further shown an approach to incorporate single Si dopants into the graphene lattice at preselected locations, localizing single-dopant atoms at specific lattice sites. Based on these studies, we aim to further develop atomic-scale control and, critically, demonstrate atom-by-atom assembly by electron beam manipulation. Here, we demonstrate the transition from single-dopant control toward the creation of a Si dimer, trimer, and tetramer from Si substitutional point defects.

While this work examines specifically Si dopants in graphene, it is worth noting that a variety of other dopants have been observed in/on graphene, including B, N,^[13,41–43] O,^[16] P,^[44,45] Fe, Au, Cr, Ti, Pd, Ni, and Al,^[46] with P also showing e-beam-induced movement through the lattice (though only a very short distance).^[44] In addition to graphene, a variety of dopants and defects have also been observed in other 2D materials which may provide other opportunities for e-beam mediated atomic alterations, for example, electron beam-induced defect production and doping in 2D transition metal dichalcogenides (TMDs).^[47–49] Such precise tailoring may enable in situ fabrication such as graphene quantum dots embedded in hexagonal boron nitride (h-BN)^[50] or graphene-based spin current diodes.^[51]

It should be mentioned that one significant enabling factor in the use of graphene for the atomic manipulation described is the high conductivity and robust resistance to beam damage at the accelerating voltage used here for manipulation (60 kV). h-BN and TMDs, for example, quickly decompose under similar irradiation. However, results from Algara-Siller et al.^[52] and Zan et al.^[53] suggest that it may be possible to stabilize such materials by encapsulation with graphene. Whether this strategy will still allow beam-induced manipulation of defects is unknown, but that some alterations were still possible under these conditions suggests that it may. This indicates that there is a possibility for extending similar techniques to other 2D materials that are of keen interest to the scientific community, as well as extending the number of atomic species available for manipulation.

2. Computational Methods

Geometry optimization of defective graphene was carried out within density functional theory (DFT), with the Perdew–Burke–Ernzerhof^[54] exchange–correlation functional and the projected augmented wave method,^[55,56] as implemented in the

Vienna *ab-initio* simulation package.^[57] We used a plane-wave kinetic energy cutoff of 520 eV and Γ centered $4 \times 8 \times 1$ k point grid. The convergence criterion was set to 10^{-5} (10^{-6}) eV for geometry (electronic) and 0.02 eV \AA^{-1} for forces. The DFT-D3 with Becke–Johnson damping scheme^[58,59] was used to account for the dispersion interactions. We first optimized the lattice of perfect graphene, resulting in a lattice constant of 2.468 \AA , and a C–C bond length of 1.425 \AA . Defective graphene was then modeled using an 8×4 unit cell, containing a total of 64 C atoms. For each Si-doped structure modeled in the present work, not only planar geometries were considered, but Si atoms were placed below and above the plane in all the possible configurations. A more accurate Γ centered $12 \times 24 \times 1$ k point grid was used for the projected density of states (PDOS).

3. Introducing Atomic-Scale Defects

The first step of e-beam fabrication of atomic structures in graphene is the controllable introduction of substitutional defects within the pristine graphene lattice. Previously, we demonstrated how single atoms or small clusters of atoms may be introduced into a graphene lattice.^[40] This approach has the advantage of highly precise positioning of the defect in the lattice. However, it is fairly slow, taking a couple of minutes per defect, and risks damaging the graphene lattice with the 100 keV beam to the point that it is unable to heal. Thus, it becomes somewhat tedious to control beam position, blanking, scanning, and imaging in such a way as to produce single defects with the care required to protect the rest of the graphene from beam damage.

In an attempt to develop a more user-friendly way of introducing point defects into the lattice we developed two alternative techniques that sacrifice the precise positioning of the previous technique but gain in ease of execution. **Figure 1** summarizes these two techniques. (a)–(d) show the first technique. In (a), a region (circled) is chosen near the source material. The e-beam is then drawn via operator control from the source material onto the pristine graphene lattice a few times (on the order of 1–3 s of total exposure time to the 100 keV electron beam), (b). This causes a repeated agitation and sputtering of the source material followed by the introduction of vacancies in the graphene lattice. This procedure decreases the likelihood of creating a large hole in the graphene that will not heal, because the beam is not left stationary. In this approach, the location of the defects created are spread over 1–2 nm in the locations over which the beam was moved. While this method appears to work fairly consistently and easily, there remains the danger of accidentally introducing large holes that will not heal. The main reason is that while the beam is under manual control in this way, imaging is not possible so real-time monitoring of the state of the sample is precluded and large holes may still be formed accidentally.

Figure 1e–h illustrates an alternative technique for the introduction of substitutional defects within a defined area. With this method, an overview image is acquired, (e), and a subscan location is selected over both the pristine graphene and source material, illustrated with the box. The subscan location may be moved around via operator control while the beam is scanning

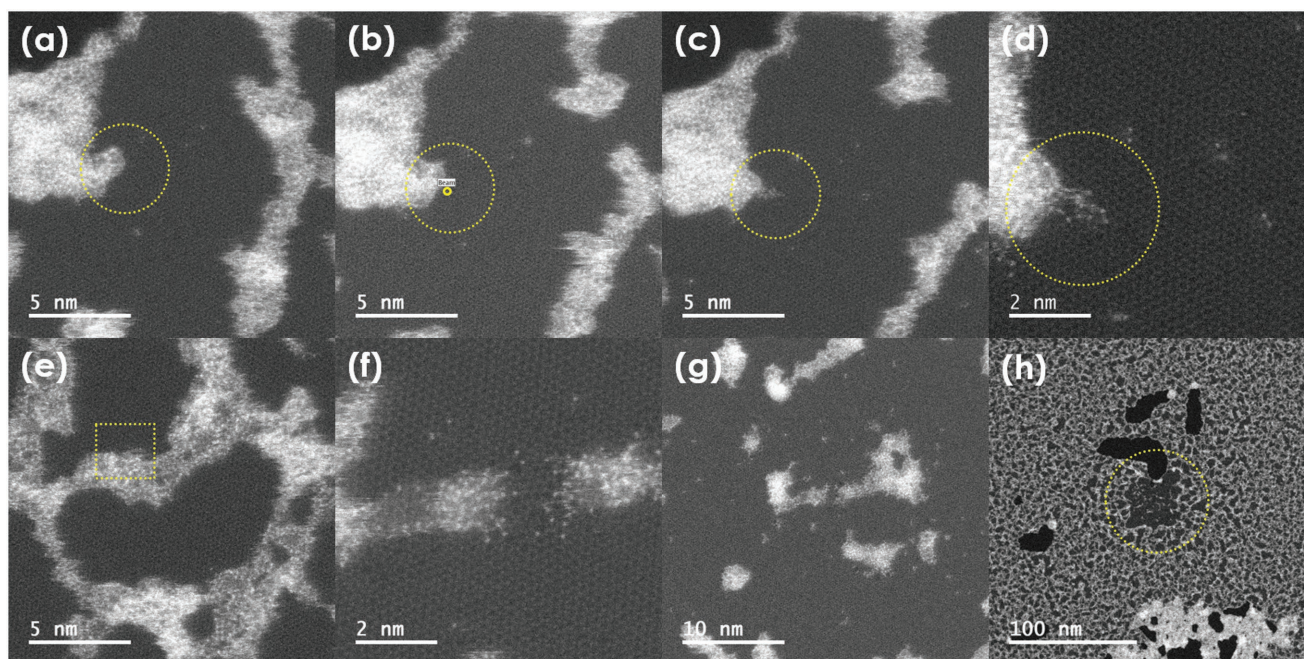


Figure 1. Introduction of Si substitutional defects and defect clusters into a graphene lattice a–d). a) An area close to the source material is chosen. b) The stationary beam is moved “by hand” over areas where defects are to be created. The small circle indicates the beam location, which was moved back and forth from the source material to the graphene. c) As atoms from the source material were introduced into the lattice we begin to see a bright area where the beam was moved. A magnified view is shown in d) where the graphene lattice and defect clusters are easily observed. e–h) show a similar but distinct way of introducing many substitutional defects from the source material. A typical area of the source material is shown in e). A subscan area is selected, as indicated by the box, and manually moved along the edges of the source material so that the graphene lattice and the source material is irradiated. This simultaneously sputters away the source material and creates vacancies in the graphene lattice which have a high likelihood of becoming passivated by a sputtered Si atom. f) A typical state after a few seconds of scanning, where many defects have been formed in the graphene lattice and much of the source material is gone. g) shows the same area as f) but at a lower magnification. h) shows a much lower magnification of the irradiated area, circled, and the surrounding web of source material.

within the subscan region. The image produced from the subscan area can then be used to monitor the state of the sample in real time. This procedure also both sputters the source material and introduces vacancies in the graphene lattice. The results of this procedure are shown at various magnifications in (f)–(h). In (f) individual substitutional Si atoms have been introduced into the graphene lattice. While it is difficult to measure exact exposure times to a specific area due to the dynamic motion of the subscan box, exposures on the order of 10–30 s are typical. A lower magnification image is shown in (g) where many defects and small clusters of defects can be seen stuck in the lattice. Finally, (h) is further demagnified to contrast the final state of the region of interest with the surrounding area. Much of the source material has been sputtered away revealing tens of nanometers of mostly pristine graphene harboring the introduced defects.

4. Extended Movement of Si-Dopant Atoms

Once the substitutional Si defects have been introduced, we can begin to explore the capabilities of an STEM for atomic level control. Movement of single Si atoms through a graphene lattice has been explored previously.^[18,29,39] Positioning the focused beam on a C atom adjacent to the Si atom results in a bond reversal where the C and Si atoms switch lattice sites.

The Si atom can, thus, be gradually moved through the lattice. A critical enabling aspect of atomic-scale manipulation in STEM will be to establish sample treatment procedures that enable extended movement of the introduced dopant atoms. To this end, here we show an example of directionally controlled atomic motion over a path length of 4.5 nm achieved on a sample using the treatment procedure described. The accelerating voltage used here was 60 kV with a convergence angle of 30 mrad and beam current of ≈ 60 pA. **Figure 2** shows a summary of the directed motion. The images were acquired with the minimum dose necessary to distinguish the lattice. They were artificially colored with the fire look up table in ImageJ and blurred with a Gaussian to aid in visibility. In a similar experiment we moved a Si atom in a circle to prevent it from moving out of the field of view and were able to achieve a total path distance of 6.5 nm. Videos of both are provided in the Supporting Information. Thus, we conclude that the sample treatment procedure has allowed imaging and manipulation over extended distances without unwanted contamination or chemically reactive elements altering the defects.

5. Formation of Silicon Dimers

The ability to move single-dopant atoms suggests that the construction of structures atom by atom is achievable via in situ

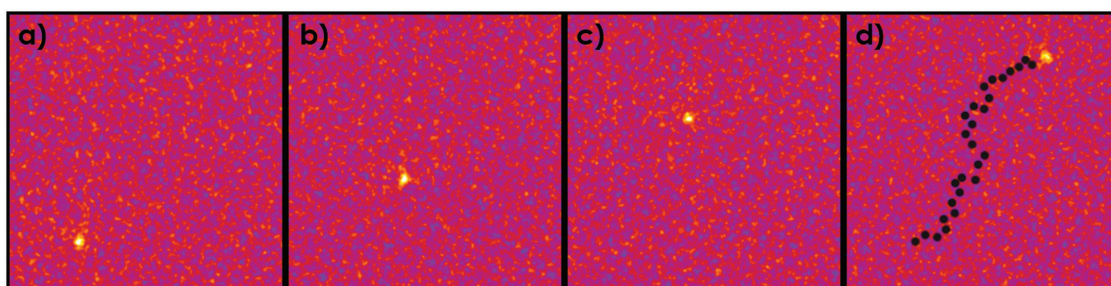


Figure 2. Illustration of beam-induced atomic motion over a path length of 4.5 nm. The focused electron beam was positioned on top of adjacent C atoms to encourage the bright Si dopant to exchange places with the irradiated neighbor. a) shows the initial configuration and b–d) show subsequent images of the progress. d) indicates the recorded lattice positions of the Si atom through time (black dots). A video of each acquired frame is presented in the Supporting Information. The field of view is 4 nm.

STEM and, here, we explore a few simple structures fabricated in this way. The results shown in Figure 1 were acquired using a 100 keV electron beam to assist in the production of defects in the graphene lattice. For the rest of the experimental results, the accelerating voltage was lowered to 60 kV to prevent continued damage and allow closer inspection of the formed defects.

Figure 3a shows a high angle annular dark field (HAADF) image of two Si substitutional point defects introduced into the lattice within close proximity of one another. Both defects exhibit threefold coordination with the carbon lattice. A small subscan area was used to direct the electron beam onto carbon atoms adjacent to the Si atoms in the desired direction of motion. A short video of the directed motion of a Si atom performed in this manner may be found in the Supporting Information. In this example, we attempted to move the upper left Si atom. The circle marks the starting location in (b)–(g) and the dotted lines record the atom's movements through time. In (d), the process of acquiring the image resulted in the unintentional movement of the lower left Si atom. In (f) the subscan area

was large enough to cause both atoms to move to the positions shown in (g). The inset in (g) shows an atomic model of the configuration at this stage. The two Si atoms are sitting opposite each other in the hexagonal ring. An attempt was made to pull them closer together by scanning over the two carbon atoms at the top of the ring, but instead, a Si atom was ejected from the lattice and the material restructured into a single Si occupying two lattice sites in the fourfold configuration, (h). Given that the majority of the beam fluence was focused onto the adjacent carbon atoms, it is likely that one of the Si atoms transitioned to one of these sites first and then, being under the beam, was ejected from the lattice. The inset in (h) shows an atomic model of the final configuration.

In order to understand more clearly the formation and stability of the structures formed in Figure 3, we performed DFT calculations of similar structures (shown in Figure 4), exploring the relaxed configurations and energies of two Si substitutional defects as they approach each other in the graphene lattice. We modeled eight configurations, starting from a Si–Si distance of

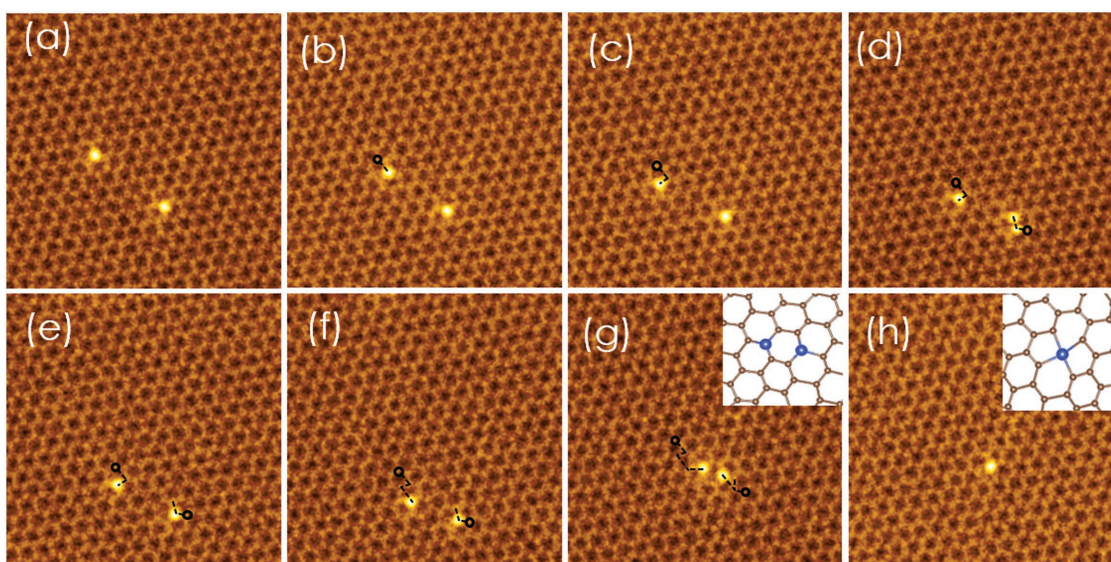


Figure 3. Creation of a Si dimer within a graphene lattice via e-beam manipulation. a) shows the starting configuration with two threefold coordinated Si atoms sitting in substitutional lattice sites. In b–g) the motion of the two Si atoms are tracked as they are moved. The original positions are indicated by the small circles and the dotted line records the atom positions through time. Between g) and h) a Si atom was ejected from the lattice (unintentionally) and the remaining Si atom became fourfold coordinated to occupy two lattice sites, accounting for the loss of an atom from the lattice.

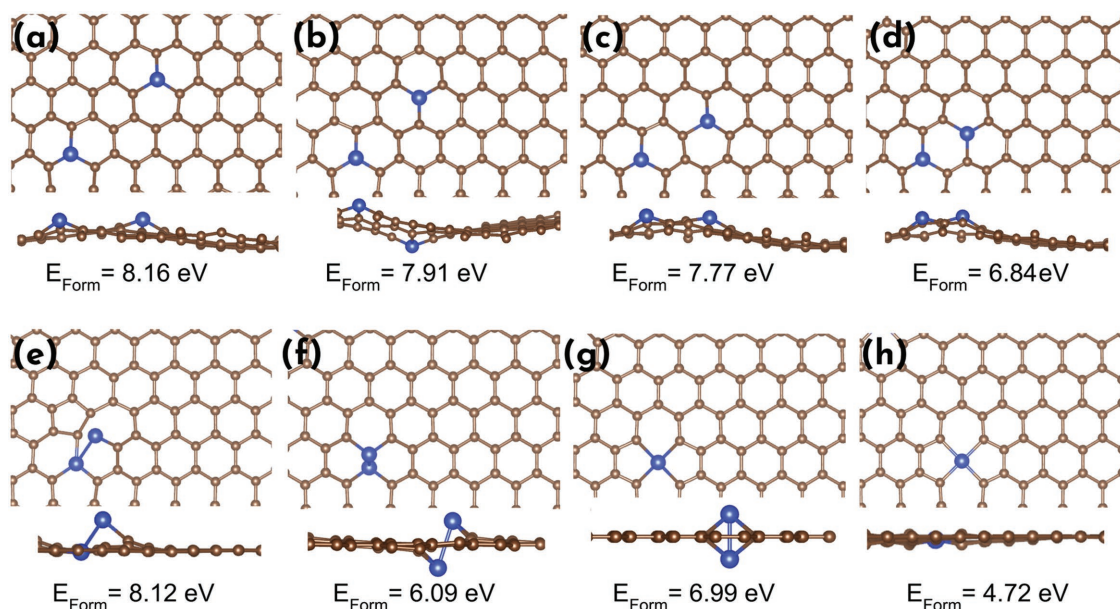


Figure 4. Final structures optimized with DFT. Si atoms are approaching each other from a) to g). For each structure a top-down view and lateral view are shown, along with the formation energy, in eV. Carbon atoms are depicted in brown and Si atoms in blue.

6.56 Å (Figure 4a), and decreasing the distance between them by one lattice site for each new configuration, (b)–(d). In (e)–(g) we modeled three stable configurations where the Si atoms are in closer proximity to each other than the structure shown in (d). By “stable” here we refer to atomic configurations that represent energetic minima that are likely candidates for experimental observation. These structures were not observed in the experiments performed here but, nevertheless, represent possible stable structures that might be observed (see, for example, Susi et al.,^[18] Supporting Information). The final structure observed experimentally is shown in (h), with one Si atom in a fourfold coordination. The optimized monolayers evidence a clear preference for corrugated structures, to the detriment of completely planar ones. This can be easily understood considering that silicon is bigger than carbon. Indeed, we find that in general, the closer the Si atoms are, the less stable becomes the planar configuration. For (f) and (g) no planar variations are stable. The formation energies of the defects were calculated as $E_{\text{Form}} = E_{\text{def}} + n\mu(\text{C}) - m\mu(\text{Si}) - E_{\text{perfect}}$, where E_{def} and E_{perfect} are the energy of the defective and perfect graphene, respectively, $\mu(\text{C})$ is the chemical potential of C, estimated as the total energy per atom in graphene, $\mu(\text{Si})$ is the chemical potential of Si, calculated from the total energy per atom of Si in the bulk Si,^[60] and n and m are the total number of C atoms removed and number of Si atoms added to the defective structure. The formation energies reveal the preference for Si atoms to be close to each other, in agreement with the results of Susi et al.^[18] presented in the Supporting Information. The formation energy decreases when going from (a) to (d), i.e., when the two Si atoms approach each other. E_{Form} , however, goes up in (e) and reaches its minimum value for (h), with just one silicon atom fourfold coordinated in the lattice. This correlates well with the experiment, since structures (e)–(g) were not observed. The relative energy for structures (d) and (h) as calculated in ref. [18], is $E_{\text{rel}} = E_{\text{form}}^{\text{h}} - E_{\text{form}}^{\text{d}} = 2.12$ eV, which means that

the structure with just one fourfold coordinated Si atom (h) is 2.12 eV more stable than the structure with two Si atoms close to each other (d). It is worth commenting on the possibility of structures (f)–(h) being that observed in Figure 3h. It is possible that the Si atoms in structure (f) would be too close together to resolve in the experiment and may appear to be just a single atom, but in this configuration, we would see an elongated bright spot in the experimental image, which does not appear to be the case. Conversely, if the configuration in (g) was captured, where the Si atoms stack on top of the other, the Si atoms would become brighter than a single Si atom. Again, this is not what we see in the experimental images. Thus, we conclude that we are observing the configuration shown in (h). Considering that we are manipulating the sample with a 60 keV electron beam, it is possible that one of the two Si atoms gained enough energy to escape from the lattice. Furthermore, due to the great affinity of silicon with oxygen, it is also possible that foreign adatoms may have chemically facilitated this process. We additionally calculated the formation energy of a similar structure to (h), but with a second Si placed at ≈ 12 Å from the lattice, representing e-beam-induced ejection from the lattice into the vacuum. This energy is 10.58 eV and can be viewed as an upper limit required for this transition given that it is likely that the ejected atom remains a loosely bound adatom which quickly diffused away from the imaged area^[61] or was involved in an additional chemical reaction with, for example, oxygen or hydrogen.

Given that Si atoms in the graphene lattice have two frequently observed coordinations, we further assembled two fourfold coordinated Si substitutional defects into a dimer with a different final structures. **Figure 5** shows a process where two fourfold coordinated Si atoms were brought together via electron beam manipulation by performing a subscan over the carbon atoms between the two Si atoms, (a)–(c). We remind the reader that the fourfold coordinated Si atoms replace two

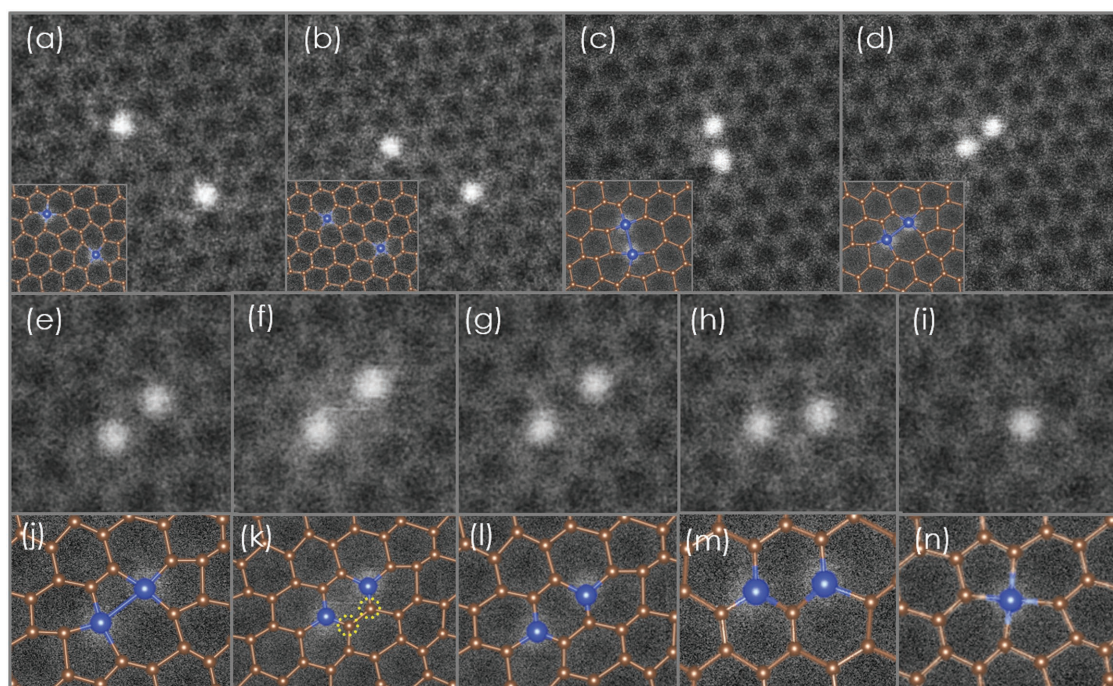


Figure 5. Creating an alternately structured Si dimer and observing an atomic-scale electron-beam-assisted chemical reaction. a–c) show the result of pulling together two fourfold coordinated Si atoms. d–i) show the evolution of the created dimer under continued e-beam irradiation. j–n) show atomic models overlaid on the images from e–i). The atomic models are based on the images only and do not represent theoretical modeling. e–i) are frames taken from a ten-frame video which may be found in the supporting information. During the acquisition of the video two additional carbon atoms are introduced into the structure, circled in k). This converts the Si atoms to threefold coordination. The right-hand Si atom moves down in h) and m) and, finally, the left-hand Si atom is ejected from the lattice in i) and n), resulting in a single fourfold coordinated Si. From c) to d), the electron beam irradiation-induced rotation of the defect. This is similar to the observations of Yang et al.^[37]

C atoms and create two adjacent pentagonal rings. As they are brought together in (c), a pentagonal ring from each of the Si defects merge to form a 5–8–5 structure.

The images shown in (e)–(i) are frames from a ten-frame video (included in the Supporting Information) with (j)–(n) showing the corresponding atomic models. The starting configuration, (e), is the same as that shown in (d). In (f) there occurred a slight blur around the Si atoms as two C atoms flew into the illuminated region and restored the lattice to hexagonal symmetry. This blur is presumably due to the structural changes associated with the incorporation of the two additional C atoms. The two new atoms are indicated by dotted circles in the atomic model, (k). In (g), the new C atoms stopped moving, the blur disappeared, and the lattice was converted to the same structure as that shown in Figure 3g, namely, two threefold coordinated Si atoms sitting opposite each other in a hexagonal ring. In (h) and (m), the right-hand Si atom moved down one lattice site and in (i) and (n) the left-hand Si atom was ejected from the lattice. The ejection of the one Si atom requires that the remaining Si atom assume a fourfold coordination to occupy two lattice sites.

6. Formation of Si Trimer And Tetramer

As a final example of e-beam assembly of nanostructures embedded in graphene we illustrate formation of a Si trimer and tetramer from a dimer of the same configuration as that

formed in Figure 5a–c. The dimer shown in **Figure 6a** was introduced into the graphene lattice via the process described at the beginning, whereby we created a host of defects in the graphene lattice. This is the same defect structure observed upon assembling two fourfold coordinated Si substitutional defects. In Figure 6b, a bond rotation was induced by the scanning electron probe involving the carbon atoms adjacent (below) the Si dimer, arrowed in the figure. This rotation likely occurs on the order of ≈ 100 fs (see Yang et al.^[37] Supporting Information and Susi et al.^[18] Video S1, Supporting Information). This is 11 orders of magnitude faster than our pixel dwell time and therefore not imageable in transition. Because the imaging process is extended through time, what we are observing is the juxtaposition of the initial configuration in the top half of the defect, before the rotation, and the final configuration on the bottom half, after the rotation. In (c), the bond rotation has completed. In (d), we observe a mobilized Si adatom has attached itself to the defect. We address how this may be accomplished later. This adatom was momentarily knocked away by the beam as shown in (e). A few moments later another adatom reattached to the implanted defect, we observe a beam-induced exchange of the two carbon atoms involved in the rotation with the Si adatom, the final configuration of which is shown in (f). Yang et al.^[37] also observed this bond rotation and acquisition of a third Si atom and provide a more in-depth discussion, which we will not repeat here. We merely repeat that this trimer can be rotated easily with the electron beam positioned on top of a carbon atom adjacent to the trimer, as shown in (g). To attach a

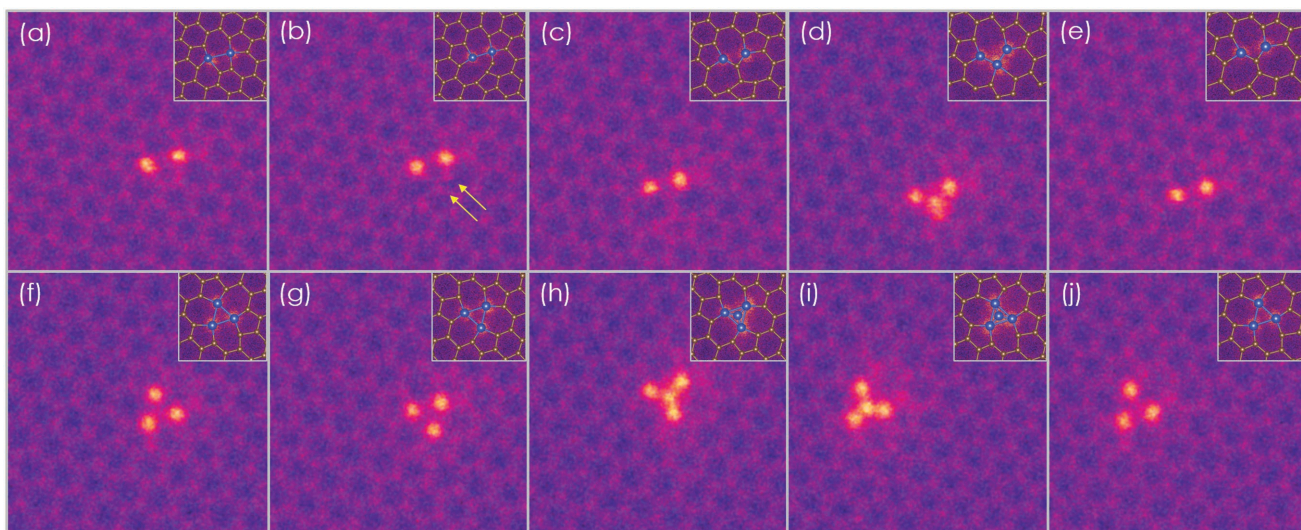


Figure 6. Evolution of a Si dimer under the influence of the 60 keV beam. Insets show the suggested atomic models based on the images (not simulation). a) shows the initial configuration. In b), we observe a bond rotation beginning to occur next to the Si dimer (arrowed). c) shows the configuration after the bond rotation has occurred. In d), we observe a Si adatom temporarily attaching to the defect. The adatom was knocked away and we return to the configuration shown in e) which appears identical to that in c). In f), an adatom is recaptured and incorporated into the lattice. Once in this configuration, all subsequent configurations, g)–j), could be repeatedly produced through electron beam manipulation. Images were artificially colored using the fire look up table in ImageJ.

fourth Si atom to the structure, (h), the beam was scanned over a large area ($\approx 50\text{--}100\text{ nm}$) to agitate and mobilize surrounding source material and adatoms. Within a few tens of seconds, the fourth Si atom was added to the structure. We suggest this method will also reproducibly attach a third Si atom to the dimer, as observed in (d). This new structure could also be rotated, shown in (i). Positioning the beam on the central Si atom lead to the ejection of this atom from the structure and a return to the trimer configuration, shown in (j). All configurations shown in (g)–(i) could be repeatedly brought about through controlled e-beam exposure. It is less clear, however, whether the bond rotation and subsequent capture and incorporation of a Si adatom is the most favorable formation pathway for the trimer structure (we have also observed trimers and tetramers formed during the dopant insertion stage). Nevertheless, given that Yang et al.^[37] observed the bond rotation to be reversible, and that the capture of the third Si atom can be intentionally directed, as evidenced by the capture of the fourth Si atom, we conclude that each of these structures can be formed through careful e-beam exposure.

Using DFT we modeled various Si-doped graphene monolayers found in Figure 6. The optimized structures are shown in Figure 7, along with the calculated formation energies. Note that from Figure 7b–c the two C atoms involved in the bond rotation were lost. For the Si trimer, Figure 7c, we found that one Si sits in-plane, a second one below and a third

above the plane, in agreement with the findings of Yang et al.^[37] In the tetramer, Figure 7d, the central Si is above the rest of the three Si atoms at a 2.38 Å distance. This is the only stable geometry we found for the tetramer observed experimentally. Interestingly, the energy required to create the Si trimer is the same as for the Si dimer in (a) and it is similar to the energy

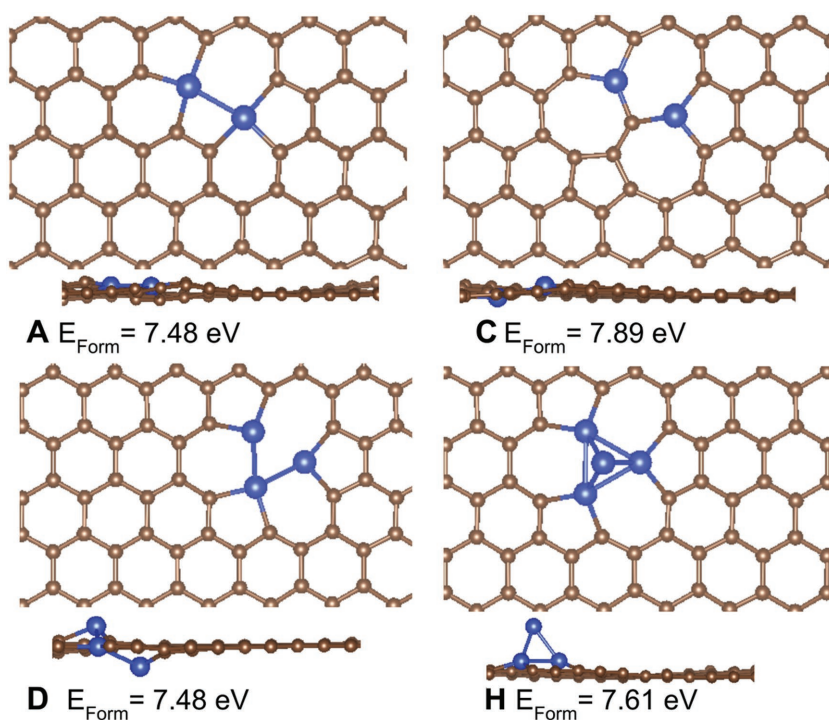


Figure 7. Calculated most stable structures observed experimentally in Figure 6. Carbon atoms are depicted in brown and Si atoms in blue.

required to create the tetramer. Finally, the partial density of states (PDOS) plots built for a variety of Si-doped graphene monolayers (see Supporting Information) show that the p_z orbitals are closer to the valence band edge.

7. Conclusion

We have shown how Si substitutional defects and Si defect clusters may be introduced into a graphene lattice via in situ STEM techniques. A prerequisite for this process is that the samples remain free of e-beam-induced hydrocarbon deposition. This is achieved through an ArO₂ annealing process which we borrowed from Garcia et al.^[62] and investigated previously.^[63] We demonstrate that directing a 100 keV focused electron beam across the source material and the graphene lattice can reliably generate multiple substitutional Si defects. Subsequent manipulation of the introduced defects may be accomplished by decreasing the microscope accelerating voltage to 60 kV and using controlled scan areas or direct stationary beam irradiation to induce movement. We showed controllable e-beam-induced formation of two Si dimers from two threefold coordinated Si substitutional atoms and two fourfold coordinated Si substitutional atoms. We also documented a formation pathway for Si trimers and tetramers, reversible conversion of a Si trimer to tetramer, and the controllable rotation of both structures. DFT modeling was performed to more clearly understand the structures formed, the energies required to form them, and explore other possible stable structures. These represent the first steps toward general atomic-scale manufacturing.

Finally, we also captured an image time-series of an atomic-scale electron-beam-assisted chemical reaction occurring with atomic resolution. As technologies such as detector efficiency, compressed sensing, and artificial intelligence improve, such observations will become more commonplace and will provide a wealth of information to enhance our understanding of atomic-scale physics and our mastery of materials. In the words of Feynman “I am not afraid to consider the final question as to whether, ultimately—in the great future—we can arrange the atoms the way we want; the very atoms, all the way down! What would happen if we could arrange the atoms one by one the way we want them.”^[1] This great future is unfolding before us.

8. Experimental Section

Graphene was grown on a Cu foil via atmosphere pressure chemical vapor deposition.^[64] The Cu foil was spin-coated with poly(methylmethacrylate) (PMMA) to form a mechanical stabilizing layer, after which the foil was dissolved away in an ammonium persulfate-deionized (DI) water solution (0.05 g mL⁻¹). The graphene/PMMA film was transferred first to hydrogen chloride diluted in DI water and then to a DI water bath for the removal of ammonium persulfate residue, followed by a final rinse in a fresh DI water bath before being transferred to a TEM grid. The graphene/PMMA film was then scooped from the bath with a TEM grid and heated on a hot plate at 150 °C for ≈20 min to make better adhesion to the grid substrate. Then, most of the PMMA was dissolved in an acetone bath, followed by an isopropyl alcohol rinse. Finally, the grid was annealed in an Ar–O₂ (450 sccm/45 sccm) environment at 500 °C for 1.5 h to mitigate hydrocarbon deposition in the microscope.^[62,63] The Si atoms examined are ubiquitously found on samples fabricated using

this and similar procedures, likely sourced from the quartz growth and baking tubes or the glassware used for sample transfer. These present themselves mixed into the residual, amorphous carbon contamination which forms the source of the Si atoms during the in situ experiments and which are referred as the “source material.”

Imaging of the sample was performed in a Nion UltraSTEM U100 at an accelerating voltage of 100 and 60 kV, as indicated in the text. At 100 kV the beam current was 30–40 pA and at 60 kV the beam current was 60–70 pA. The medium angle annular dark field detector was used for imaging at 100 kV to enhance image contrast and the HAADF detector was used for imaging at 60 kV in order to preserve Z-contrast.^[65] Voltage changes were performed at the end of the day and work resumed the following morning to allow ample time for the objective lens to reach thermal stability.

Supporting Information

Supporting Information is available from the Wiley Online Library.

Acknowledgements

The authors would like to thank Dr. Ivan Vlasiouk for provision of the graphene samples and Dr. Francois Amet for assistance with the argon–oxygen cleaning procedure. Research was performed at the Center for Nanophase Materials Sciences, which is a US Department of Energy Office of Science User facility. Experimental work was supported by the Laboratory Directed Research and Development Program of Oak Ridge National Laboratory, managed by UT-Battelle, LLC for the U.S. Department of Energy (O.D., S.K., S.V.K., S.J.).

Conflict of Interest

The authors declare no conflict of interest.

Keywords

atomic control, electron beam, graphene, scanning transmission electron microscope, silicon dimer

Received: May 8, 2018
Revised: July 24, 2018
Published online: August 26, 2018

- [1] R. P. Feynman, *Eng. Sci.* **1960**, 23, 22.
- [2] G. Binnig, H. Rohrer, *Helv. Phys. Acta* **1982**, 55, 726.
- [3] G. Binnig, H. Rohrer, (Google Patents), Scanning tunneling microscope, *US4343993A*, **1982**.
- [4] G. Binnig, H. Rohrer, *Rev. Mod. Phys.* **1987**, 59, 615.
- [5] D. M. Eigler, E. K. Schweizer, *Nature* **1990**, 344, 524.
- [6] D. M. Eigler, C. P. Lutz, W. E. Rudge, *Nature* **1991**, 352, 600.
- [7] M. F. Crommie, C. P. Lutz, D. M. Eigler, *Nature* **1993**, 363, 524.
- [8] M. F. Crommie, C. P. Lutz, D. M. Eigler, *Science* **1993**, 262, 218.
- [9] M. Fuechsle, J. A. Miwa, S. Mahapatra, H. Ryu, S. Lee, O. Warschkow, L. C. L. Hollenberg, G. Klimeck, M. Y. Simmons, *Nat. Nanotechnol.* **2012**, 7, 242.
- [10] B. Weber, S. Mahapatra, H. Ryu, S. Lee, A. Fuhrer, T. C. G. Reusch, D. L. Thompson, W. C. T. Lee, G. Klimeck, L. C. L. Hollenberg, M. Y. Simmons, *Science* **2012**, 335, 64.
- [11] S. R. Schofield, N. J. Curson, M. Y. Simmons, F. J. Rueß, T. Hallam, L. Oberbeck, R. G. Clark, *Phys. Rev. Lett.* **2003**, 91, 136104.

- [12] A. V. Krasheninnikov, K. Nordlund, *J. Appl. Phys.* **2010**, *107*, 071301.
- [13] T. Susi, J. Kotakoski, R. Arenal, S. Kurasch, H. Jiang, V. Skakalova, O. Stephan, A. V. Krasheninnikov, E. I. Kauppinen, U. Kaiser, J. C. Meyer, *ACS Nano* **2012**, *6*, 8837.
- [14] J. C. Meyer, C. Kisielowski, R. Erni, M. D. Rossell, M. F. Crommie, A. Zettl, *Nano Lett.* **2008**, *8*, 3582.
- [15] A. Zobelli, A. Gloter, C. P. Ewels, G. Seifert, C. Colliex, *Phys. Rev. B* **2007**, *75*, 245402.
- [16] R. Zan, Q. M. Ramasse, U. Bangert, K. S. Novoselov, *Nano Lett.* **2012**, *12*, 3936.
- [17] J. C. Meyer, F. Eder, S. Kurasch, V. Skakalova, J. Kotakoski, H. J. Park, S. Roth, A. Chuvilin, S. Eyhusen, G. Benner, A. V. Krasheninnikov, U. Kaiser, *Phys. Rev. Lett.* **2012**, *108*, 196102.
- [18] T. Susi, J. Kotakoski, D. Kepaptsoglou, C. Mangler, T. C. Lovejoy, O. L. Krivanek, R. Zan, U. Bangert, P. Ayala, J. C. Meyer, Q. Ramasse, *Phys. Rev. Lett.* **2014**, *113*, 115501.
- [19] J. Kotakoski, J. C. Meyer, S. Kurasch, D. Santos-Cottin, U. Kaiser, A. V. Krasheninnikov, *Phys. Rev. B* **2011**, *83*, 245420.
- [20] I. Gonzalez-Martinez, A. Bachmatiuk, V. Bezugly, J. Kunstmann, T. Gemming, Z. Liu, G. Cuniberti, M. Rummeli, *Nanoscale* **2016**, *8*, 11340.
- [21] A. Ramasubramaniam, D. Naveh, *Phys. Rev. B* **2011**, *84*, 075405.
- [22] W. F. V. Dorp, X. Zhang, B. L. Feringa, J. B. Wagner, T. W. Hansen, J. T. M. D. Hosson, *Nanotechnology* **2011**, *22*, 505303.
- [23] T. Susi, D. Kepaptsoglou, Y.-C. Lin, Q. M. Ramasse, J. C. Meyer, K. Suenaga, J. Kotakoski, *2D Mater.* **2017**, *4*, 042004.
- [24] S. Jesse, A. Y. Borisevich, J. D. Fowlkes, A. R. Lupini, P. D. Rack, R. R. Unocic, B. G. Sumpter, S. V. Kalinin, A. Belianinov, O. S. Ovchinnikova, *ACS Nano* **2016**, *10*, 5600.
- [25] S. Jesse, Q. He, A. R. Lupini, D. N. Leonard, M. P. Oxley, O. Ovchinnikov, R. R. Unocic, A. Tselev, M. Fuentes-Cabrera, B. G. Sumpter, S. J. Pennycook, S. V. Kalinin, A. Y. Borisevich, *Small* **2015**, *11*, 5895.
- [26] S. V. Kalinin, A. Borisevich, S. Jesse, *Nature* **2016**, *539*, 485.
- [27] N. Jiang, E. Zarkadoula, P. Narang, A. Maksov, I. Kravchenko, A. Borisevich, S. Jesse, S. V. Kalinin, *MRS Bull.* **2017**, *42*, 653.
- [28] S. V. Kalinin, S. J. Pennycook, *MRS Bull.* **2017**, *42*, 637.
- [29] T. Susi, J. C. Meyer, J. Kotakoski, *Ultramicroscopy* **2017**, *180*, 163.
- [30] J. Kotakoski, D. Santos-Cottin, A. V. Krasheninnikov, *ACS Nano* **2012**, *6*, 671.
- [31] Q. M. Ramasse, C. R. Seabourne, D.-M. Kepaptsoglou, R. Zan, U. Bangert, A. J. Scott, *Nano Lett.* **2013**, *13*, 4989.
- [32] Z. He, K. He, A. W. Robertson, A. I. Kirkland, D. Kim, J. Ihm, E. Yoon, G.-D. Lee, J. H. Warner, *Nano Lett.* **2014**, *14*, 3766.
- [33] A. W. Robertson, G.-D. Lee, K. He, Y. Fan, C. S. Allen, S. Lee, H. Kim, E. Yoon, H. Zheng, A. I. Kirkland, J. H. Warner, *Nano Lett.* **2015**, *15*, 5950.
- [34] A. W. Robertson, G.-D. Lee, K. He, E. Yoon, A. I. Kirkland, J. H. Warner, *Nano Lett.* **2014**, *14*, 1634.
- [35] A. W. Robertson, G.-D. Lee, K. He, E. Yoon, A. I. Kirkland, J. H. Warner, *Nano Lett.* **2014**, *14*, 3972.
- [36] A. W. Robertson, B. Montanari, K. He, J. Kim, C. S. Allen, Y. A. Wu, J. Olivier, J. Neethling, N. Harrison, A. I. Kirkland, J. H. Warner, *Nano Lett.* **2013**, *13*, 1468.
- [37] Z. Yang, L. Yin, J. Lee, W. Ren, H.-M. Cheng, H. Ye, S. T. Pantelides, S. J. Pennycook, M. F. Chisholm, *Angew. Chem.* **2014**, *126*, 9054.
- [38] J. Lee, W. Zhou, S. J. Pennycook, J.-C. Idrobo, S. T. Pantelides, **2013**, *4*, 1650, <https://www.nature.com/articles/ncomms2671#supplementary-information>.
- [39] J. Lee, Z. Yang, W. Zhou, S. J. Pennycook, S. T. Pantelides, M. F. Chisholm, *Proc. Natl. Acad. Sci.* **2014**, *111*, 7522.
- [40] O. Dyck, S. Kim, S. V. Kalinin, S. Jesse, *Appl. Phys. Lett.* **2017**, *111*, 113104.
- [41] R. J. Nicholls, A. T. Murdock, J. Tsang, J. Britton, T. J. Pennycook, A. Koós, P. D. Nellist, N. Grobert, J. R. Yates, *ACS Nano* **2013**, *7*, 7145.
- [42] D. Usachov, O. Vilkov, A. Grüneis, D. Haberer, A. Fedorov, V. K. Adamchuk, A. B. Preobrajenski, P. Dudin, A. Barinov, M. Oehzelt, C. Laubschat, D. V. Vyalikh, *Nano Lett.* **2011**, *11*, 5401.
- [43] Y. Gong, G. Shi, Z. Zhang, W. Zhou, J. Jung, W. Gao, L. Ma, Y. Yang, S. Yang, G. You, R. Vajtai, Q. Xu, A. H. MacDonald, B. I. Yakobson, J. Lou, Z. Liu, P. M. Ajayan, *Nat. Commun.* **2014**, *5*, 3193, <https://www.nature.com/articles/ncomms4193#supplementary-information>.
- [44] C. Su, M. Tripathi, Q.-B. Yan, Z. Wang, Z. Zhang, L. Basile, G. Su, M. Dong, J. Kotakoski, J. Kong, J.-C. Idrobo, T. Susi, J. Li, *ArXiv e-prints* **2018**, <http://adsabs.harvard.edu/abs/2018arXiv180301369S>.
- [45] T. Susi, T. P. Hardcastle, H. Hofsässs, A. Mittelberger, T. J. Pennycook, C. Mangler, R. Drummond-Brydson, A. J. Scott, J. C. Meyer, J. Kotakoski, *2D Mater.* **2017**, *4*, 021013.
- [46] Q. M. Ramasse, R. Zan, U. Bangert, D. W. Boukhvalov, Y.-W. Son, K. S. Novoselov, *ACS Nano* **2012**, *6*, 4063.
- [47] H.-P. Komsa, J. Kotakoski, S. Kurasch, O. Lehtinen, U. Kaiser, A. V. Krasheninnikov, *Phys. Rev. Lett.* **2012**, *109*, 035503.
- [48] W. Zhou, X. Zou, S. Najmaei, Z. Liu, Y. Shi, J. Kong, J. Lou, P. M. Ajayan, B. I. Yakobson, J.-C. Idrobo, *Nano Lett.* **2013**, *13*, 2615.
- [49] J. Hong, Z. Hu, M. Probert, K. Li, D. Lv, X. Yang, L. Gu, N. Mao, Q. Feng, L. Xie, J. Zhang, D. Wu, Z. Zhang, C. Jin, W. Ji, X. Zhang, J. Yuan, Z. Zhang, *Nat. Commun.* **2015**, *6*, 6293, <https://www.nature.com/articles/ncomms7293#supplementary-information>.
- [50] J. Li, V. B. Shenoy, *Appl. Phys. Lett.* **2011**, *98*, 013105.
- [51] H. Da, Y. P. Feng, G. Liang, *J. Phys. Chem. C* **2011**, *115*, 22701.
- [52] G. Algara-Siller, S. Kurasch, M. Sedighi, O. Lehtinen, U. Kaiser, *Appl. Phys. Lett.* **2013**, *103*, 203107.
- [53] R. Zan, Q. M. Ramasse, R. Jalil, T. Georgiou, U. Bangert, K. S. Novoselov, *ACS Nano* **2013**, *7*, 10167.
- [54] J. P. Perdew, K. Burke, M. Ernzerhof, *Phys. Rev. Lett.* **1996**, *77*, 3865.
- [55] P. E. Blöchl, *Phys. Rev. B* **1994**, *50*, 17953.
- [56] G. Kresse, D. Joubert, *Phys. Rev. B* **1999**, *59*, 1758.
- [57] G. Kresse, J. Hafner, *Phys. Rev. B* **1993**, *47*, 558.
- [58] S. Grimme, J. Antony, S. Ehrlich, H. Krieg, *J. Chem. Phys.* **2010**, *132*, 154104.
- [59] S. Grimme, S. Ehrlich, L. Goerigk, *J. Comput. Chem.* **2011**, *32*, 1456.
- [60] A. Elliot, *Acta Crystallogr., Sect. B: Struct. Sci.* **2010**, *66*, 271.
- [61] Y. Yong, X. Hao, C. Li, X. Li, T. Li, H. Cui, S. Lv, *RSC Adv.* **2015**, *5*, 38680.
- [62] A. G. F. Garcia, M. Neumann, F. Amet, J. R. Williams, K. Watanabe, T. Taniguchi, D. Goldhaber-Gordon, *Nano Lett.* **2012**, *12*, 4449.
- [63] O. Dyck, S. Kim, S. V. Kalinin, S. Jesse, *J. Vac. Sci. Technol., B: Nanotechnol. Microelectron.: Mater., Process., Meas., Phenom.* **2017**, *36*, 011801.
- [64] I. Vlassiouk, P. Fulvio, H. Meyer, N. Lavrik, S. Dai, P. Datskos, S. Smirnov, *Carbon* **2013**, *54* (Supplement C), 58.
- [65] S. J. Pennycook, P. D. Nellist, *Scanning Transmission Electron Microscopy: Imaging and Analysis*, Springer Science & Business Media, Cambridge, UK **2011**.